

Propagation properties of radially polarized Pearcey-Gauss vortex beams in free space

Xinpeng Chen(陈鑫鹏), Chuangjie Xu(许创杰), Qian Yang(杨芊), Zhiming Luo(罗智明), Xixian Li(李希贤), Dongmei Deng(邓冬梅)

Citation: Chin. Phys. B . 2020, 29(6): 064202 . **doi:** 10.1088/1674-1056/ab8202
Journal homepage: http://cpb.iphy.ac.cn; http://iopscience.iop.org/cpb

What follows is a list of articles you may be interested in

Trajectory engineering via a space-fractional Schrödinger equation with dynamic linear index potential

Yunji Meng(孟云吉), Youwen Liu(刘友文), Haijiang Lv(吕海江)

Chin. Phys. B . 2020, 29(5): 054201 . **doi:** 10.1088/1674-1056/ab7b4c

Paraxial propagation of cosh-Airy vortex beams in chiral medium

Xiao-Jin Yang(杨小锦), Zhen-Sen Wu(吴振森), Tan Qu(屈檀)

Chin. Phys. B . 2020, 29(3): 034201 . **doi:** 10.1088/1674-1056/ab683f

Dielectric or plasmonic Mie object at air-liquid interface: The transferred and the traveling momenta of photon

M R C Mahdy, Hamim Mahmud Rivy, Ziaur Rahman Jony, Nabila Binte Alam, Nabila Masud, Golam Dastegir Al Quaderi, Ibraheem Muhammad Moosa, Chowdhury Mofizur Rahman, M Sohel Rahman

Chin. Phys. B . 2020, 29(1): 014211 . **doi:** 10.1088/1674-1056/ab5efa

Broadband visible light absorber based on ultrathin semiconductor nanostructures

Lin-Jin Huang(黄林锦), Jia-Qi Li(李嘉麒), Man-Yi Lu(卢漫仪), Yan-Quan Chen(陈彦权), Hong-Ji Zhu(朱宏基), Hai-Ying Liu(刘海英)

Chin. Phys. B . 2020, 29(1): 014201 . **doi:** 10.1088/1674-1056/ab5787

Comparison of three kinds of polarized Bessel vortex beams propagating through uniaxial anisotropic media

Jia-Wei Liu(刘佳伟), Hai-Ying Li(李海英), Wei Ding(丁炜), Lu Bai(白璐), Zhen-Sen Wu(吴振森), Zheng-Jun Li(李正军)

Chin. Phys. B . 2019, 28(9): 094214 . **doi:** 10.1088/1674-1056/ab37f5

Propagation properties of radially polarized Pearcey–Gauss vortex beams in free space*

Xinpeng Chen(陈鑫鹏)[1], Chuangjie Xu(许创杰)[2], Qian Yang(杨芊)[1], Zhiming Luo(罗智明)[1], Xixian Li(李希贤)[1], and Dongmei Deng(邓冬梅)[1,†]

[1] *Guangdong Provincial Key Laboratory of Nanophotonic Functional Materials and Devices, South China Normal University, Guangzhou* 510631, *China*
[2] *School of Physics, Sun Yat-Sen University, Guangzhou* 510275, *China*

(Received 3 January 2020; revised manuscript received 9 February 2020; accepted manuscript online 23 March 2020)

We investigate a family of radially polarized Pearcey–Gauss vortex beams (RPPGVBs), obtain the general propagation expressions of an RPPGVB, and study the intensity distribution, phase pattern, spin currents as well as the orbital currents when the RPPGVB propagates in free space. The focal plane and the intensity of the focal point can be adjusted by changing the position of the vortex and the scaling factors. We also investigate how the waist size influences the propagation properties.

Keywords: Pearcey–Gauss beam, propagation properties

PACS: 42.25.Bs, 42.25.Fx **DOI:** 10.1088/1674-1056/ab8202

1. Introduction

Recently, the vortex beams which contain the phase singularity have attracted much attention,[1–14] and some of their interesting properties are revealed. For instance, Gahagan and Swartzlander have demonstrated three-dimensional radiation pressure trapping of a low-index (hollow) spherical particle in water using a Gaussian beam containing an optical vortex.[1] The work of Ng *et al.* suggested that particles trapped by optical vortices must be stabilized by ambient damping.[3] What's more, Soskin *et al.* have studied the transformations of topological charge during propagation in free space and established the general rule for angular-momentum density distribution of a vortex beam within a Gaussian envelope.[4] The accesses to generating vortex beams have been researched as well including computer-generated holograms,[5] two cascaded metasurfaces,[6] three-plane-wave interference, and so on.[7–10] Up to date, the vortex beams have been applied in many areas such as carrying information, trapping and guiding particles.[11–14]

Laser beams with radial polarization have attracted widespread attention.[15–20] They are featured by a totally symmetrical electric field in which the electric vector is radially distributed along the beam axis.[15] Radially polarized beams are sharply focused light beams and can be applied in some optical instruments and devices such as lithography and confocal microscopy.[16] In addition, radially polarized beams have a higher efficiency than the plane p-polarized and circularly polarized beams in the area of the laser cutting.[17] There are also various studies on generation of radially polarized beams. For example, Machavariani *et al.* have introduced a transformation of a linearly polarized Gaussian beam to a radially polarized doughnut (0,1)* Laguerre–Gaussian beam of high purity.[18] Moreover, Yonezawa *et al.* have achieved success by use of a laser resonator including a *c*-cut Nd:YVO_4 crystal as the laser medium.[20]

On the other hand, beams with special functions, such as Airy beams and Bessel beams, have been widely investigated recently.[21–23] The Pearcey beams, based on the Pearcey function, were firstly illustrated by Pearcey in 1946. However, they have not attracted much attention until these years. In 2012, Ring *et al.* described the theory of Pearcey beams' propagation and presented experimental verification of their autofocusing and self-healing behavior.[24] Afterwards, Deng *et al.* demonstrated the virtual source of a Pearcey beam.[25] Ren *et al.* introduced dual Pearcey (DP) beams based on the Pearcey function of catastrophe theory.[26] However, generating and studying Pearcey beams experimentally are not easy because of the infinite size of Pearcey beams' cross sections. Scientists tend to add a Gaussian envelope to a Pearcey beam and obtain the Pearcey–Gauss beam. The characteristics of Pearcey–Gauss beams such as the propagation properties and vectorial structures have been revealed well by researchers.[24,27] Although theories about the properties of beams mentioned above are numerous, there are few reports on propagation properties of a radially polarized Pearcey–Gauss vortex beam (RPPGVB). Thus, we introduce this beam and investigate its propagation properties. The intensity pattern, phase pattern, spin currents and orbital currents of an RPPGVB propagating in free space are involved in our discussion.

*Project supported by the National Natural Science Foundation of China (Grant Nos. 11775083 and 11374108) and the National Training Program of Innovation and Entrepreneurship for Undergraduates, China.

†Corresponding author. E-mail: dmdeng@263.net

© 2020 Chinese Physical Society and IOP Publishing Ltd

The structure of this work is as follows. In Section 2, we derive general propagation expressions of an RPPGVB by solving the paraxial propagation equations and find out the factors influencing the propagation of the RPPGVB. Then we elicit some conclusions based on those expressions. In Section 3, we present and analyze multifarious patterns including intensity patterns, phase patterns as well as the patterns of spin currents and orbital currents, which are helpful for building deeper understanding of an RPPGVB. Finally, we draw the conclusion in Section 4.

2. Establishment and analysis of free-space propagation expressions of an RPPGVB

We assume that the RPPGVB propagates along the z-axis in the Cartesian coordinate system. At $z=0$, the electric field of the RPPGVB can be expressed as

$$\begin{aligned}\boldsymbol{E}_{0x}(x_0,y_0,0) &= \frac{x_0}{x'}\mathrm{Pe}\left(\frac{x_0}{x'},\frac{y_0}{y'}\right)\exp\left(-\frac{x_0^2+y_0^2}{w_0^2}\right)\\ &\times\left[\frac{x_0-x_\mathrm{d}}{x'}+\frac{i(y_0-y_\mathrm{d})}{y'}\right]\boldsymbol{e}_x, \qquad (1)\\ \boldsymbol{E}_{0y}(x_0,y_0,0) &= \frac{y_0}{y'}\mathrm{Pe}\left(\frac{x_0}{x'},\frac{y_0}{y'}\right)\exp\left(-\frac{x_0^2+y_0^2}{w_0^2}\right)\\ &\times\left[\frac{x_0-x_\mathrm{d}}{x'}+\frac{i(y_0-y_\mathrm{d})}{y'}\right]\boldsymbol{e}_y, \qquad (2)\end{aligned}$$

where x' and y' are scaling factors, w_0 is the waist radius of the RPPGVB, x_d and y_d describe the transfer in the x and y directions, respectively. What's more, $\mathrm{Pe}(x_0/x',y_0/y')$ represents a Pearcey function. Generally, the Pearcey function is taken as the following integral representation:[24,28]

$$\mathrm{Pe}(x,y)=\int_{-\infty}^{+\infty}\mathrm{d}s\exp\left[\mathrm{i}\left(s^4+s^2y+sx\right)\right]. \qquad (3)$$

On the other hand, in the case of paraxial approximation, the propagation expressions of the RPPGVB in free space conform the following equations:[29,30]

$$\begin{aligned}E_x(x,y,z) &= -\frac{\mathrm{i}k}{2\pi z}\exp(-\mathrm{i}kz)\int_{-\infty}^{+\infty}\int_{-\infty}^{+\infty}E_{0x}(x_0,y_0,0)\\ &\times\exp\left\{\frac{\mathrm{i}k}{2z}\left[(x-x_0)^2+(y-y_0)^2\right]\right\}\mathrm{d}x_0\mathrm{d}y_0, \qquad (4)\\ E_y(x,y,z) &= -\frac{\mathrm{i}k}{2\pi z}\exp(-\mathrm{i}kz)\int_{-\infty}^{+\infty}\int_{-\infty}^{+\infty}E_{0y}(x_0,y_0,0)\\ &\times\exp\left\{\frac{\mathrm{i}k}{2z}\left[(x-x_0)^2+(y-y_0)^2\right]\right\}\mathrm{d}x_0\mathrm{d}y_0, \qquad (5)\end{aligned}$$

where $k=2\pi/\lambda$ denotes the wavenumber, λ is the wavelength, and z is the propagation distance. We are able to obtain the propagation expressions of the RPPGVB in free space by substituting Eqs. (1) and (2) into Eqs. (4) and (5)

$$\begin{aligned}&E_x(x,y,z)\\ &= -\frac{\mathrm{i}k}{2z}M^2\exp\left[\mathrm{i}kz+\left(T+T^2M\right)\left(x^2+y^2\right)\right]\\ &\times\left\{-\frac{\mathrm{i}z^2}{k^2x'y'}\frac{1}{M}\frac{\partial^2}{\partial x\partial y}\mathrm{Pe}(X,Y)\right.\\ &+\left(\frac{x}{x'^2}+\frac{\mathrm{i}y}{2x'y'}+\frac{1}{2x'}\frac{Q}{TM}\right)\\ &\times\frac{\partial}{\partial x}\mathrm{Pe}(X,Y)+\left(\frac{\mathrm{i}x}{2x'y'}-\frac{y'z}{2kx'^4}\right)\frac{\partial}{\partial y}\mathrm{Pe}(X,Y)\\ &\left.+\left(\frac{1}{2x'^2}+\frac{x^2}{x'^2}MT^2+\frac{x}{x'}QT-\frac{xy}{2zx'y'}MT\right)\mathrm{Pe}(X,Y)\right\}, \qquad (6)\\ &E_y(x,y,z)\\ &= -TM^2\exp\left[\mathrm{i}kz+\left(T+T^2M\right)\left(x^2+y^2\right)\right]\\ &\times\left[\frac{\mathrm{i}}{4y'^2}\frac{1}{MT^2}\frac{\partial^2}{\partial y^2}\mathrm{Pe}\left(X',Y'\right)\right.\\ &+\frac{1}{4x'y'}\frac{1}{MT^2}\frac{\partial^2}{\partial x\partial y}\mathrm{Pe}\left(X',Y'\right)+\frac{y}{2x'y'}\frac{\partial}{\partial x}\mathrm{Pe}\left(X',Y'\right)\\ &+\left(\frac{x}{2x'y'}+\frac{\mathrm{i}y}{y'^2}+\frac{1}{2y'}\frac{Q}{MT}\right)\frac{\partial}{\partial y}\mathrm{Pe}\left(X',Y'\right)\\ &\left.+\left(\frac{xy}{x'y'}MT^2+\frac{\mathrm{i}y^2}{y'^2}MT^2+\frac{y}{y'}QT+\frac{\mathrm{i}}{2y'^2}\right)\mathrm{Pe}\left(X',Y'\right)\right], \qquad (7)\end{aligned}$$

where

$$M=\frac{1}{\frac{1}{w_0^2}-\frac{\mathrm{i}k}{2z}},\quad T=\frac{\mathrm{i}k}{2z},\quad Q=\frac{x_\mathrm{d}}{x'}+\frac{\mathrm{i}y_\mathrm{d}}{y'},$$

with

$$\begin{aligned}X&=-\frac{x}{x'}TM\left(1+\frac{\mathrm{i}}{4y'^2}M\right)^{-1/4},\\ Y&=\left(\frac{\mathrm{i}}{4y'^2}M-\frac{y}{y'}MT\right)\left(1+\frac{\mathrm{i}}{4y'^2}M\right)^{-1/2},\\ X'&=-\frac{x}{x'}TM\left(1+\frac{\mathrm{i}}{4y'^2}M\right)^{-1/4},\\ Y'&=\mathrm{i}M\left(\mathrm{i}Ty+\frac{1}{4x'^2}\right)\left(1+\frac{\mathrm{i}}{4y'^2}M\right)^{-1/2}.\end{aligned}$$

According to Eqs. (6) and (7), we are able to obtain the solutions to describe singularities of E_x and E_y by presuming $E_xE_y\to\infty$. Then we find the solutions also to make $XYX'Y'$ infinite. The expressions of XYX' and Y' present a common feature that there is a polynomial whose exponent is negative. If we assume x, y and z to be all finite values, those polynomials with a negative exponent will be infinite. Finally, we can list the following equation for E_x and E_y:

$$1+\frac{\mathrm{i}}{4y'^2}\left(\frac{1}{w_0^2}-\frac{\mathrm{i}k}{2z}\right)^{-1}=0. \qquad (8)$$

From Eq. (8), we find the existence condition and the position of singularity for E_x and E_y: $y'\ll w_0$ and $z=2ky'^2$.

From the above equations, we know that the RPPGVB focuses at $z=2ky'^2$ when it propagates in free space and we take this distance as z_e. What's more, when $X=Y=0$, we can obtain $\Delta x_1=0$ and $\Delta y_1=y'z/(2kx'^2)$, which represent the displacements of the beam from the initial position in the x-

and y-direction, respectively, for E_x. Displacements for E_y can be expressed as $\Delta x_2 = 0$ and $\Delta y_2 = y'z/(2kx'^2)$.

The four displacements imply that the x-component of the RPPGVB never displaces while the y-component has the same displacements for the x- and y-components.

3. Propagation properties of the RPPGVB

Figure 1 is the intensity profile of the RPPGVB at different planes as z increases in free space. When the propagation distance is not very long, there is one vortex in the central part of the profile and two faculae above the bands of main lobes. When z continues to increase, another vortex and two faculae form below the light lobes, as shown in Fig. 1(c). The vortexes expand while the faculae shrink until $z = z_e$, where the RPPGVB focuses at a point where $x = y = 0$. When $z > z_e$, the intensity pattern reverses. From Fig. 1, we also find that the energy of the RPPGVB primarily distributes on the main lobes while a little energy distributes on the other parts including the side lobes and faculae. This effect is even more apparent when the propagation distance approaches z_e. What is more, the peak intensity increases firstly before $z = z_e$ and then decreases as z increases.

Figure 2 depicts the intensity of the RPPGVB at $z = 0.5z_e$ in free space with changing x' and y'. It is quite clear that the RPPGVB's profile shifts along the negative y-direction as scaling factors x' and y' increase. Meanwhile, the maximum value of the intensity decreases rapidly and the lobes of the RPPGVB become more distinct with the intensity range becoming smaller. When scaling factors reach a certain size, $x' = y' = 0.4$ mm, for example, the shape of overall RPPGVB's cross section will become blurred, as shown in Fig. 2(f).

All parameters of Fig. 3 are the same as those in Fig. 2 except that the propagation distance equals z_e. It is apparent that the RPPGVB focuses at $z = z_e$ when the scaling factors are relatively small. From Figs. 3(a)–3(f), it is interesting that the focusing effect is the strongest when $x' = y' = 0.05$ mm. If we keep increasing the scaling factors, the focal point will disappear while the energy still gathers around the center of the beam's profile. What's more, it is shown in Figs. 3(a)–3(f) that the peak of the intensity gradually decreases to a very small value as the scaling factors increase. Comparing Fig. 3(a) with Fig. 3(f), it is also easy for us to learn that the peak intensity with $x' = y' = 0.04$ mm is almost thirty thousand times as large as that with $x' = y' = 0.05$ mm.

Figure 4 exhibits the intensity of the RPPGVB with different waist sizes in free space. When $w_0 = 0.4$ mm, there are only three bright spots where the energy concentrates in the RPPGVB's cross section. However, the whole cross section as well as the facula enlargers and the pattern of the intensity distribution is more and more obvious as w_0 gradually increases, which is presented by Figs. 4(b)–4(f). Moreover, in Fig. 4, the peak of the intensity exhibits increasing with an enlarging waist. Interestingly, from the peak intensities shown in Fig. 4, we also find that the increased rate gradually decreases as w_0 grows linearly. For example, the peak intensity for $w_0 = 0.6$ mm is five times as large as that for $w_0 = 0.4$ mm. However, the multiple reduces to 3 when w_0 changes from 0.6 mm to 0.8 mm, which even decreases to 1.8 when w_0 changes from 1.2 mm to 1.4 mm.

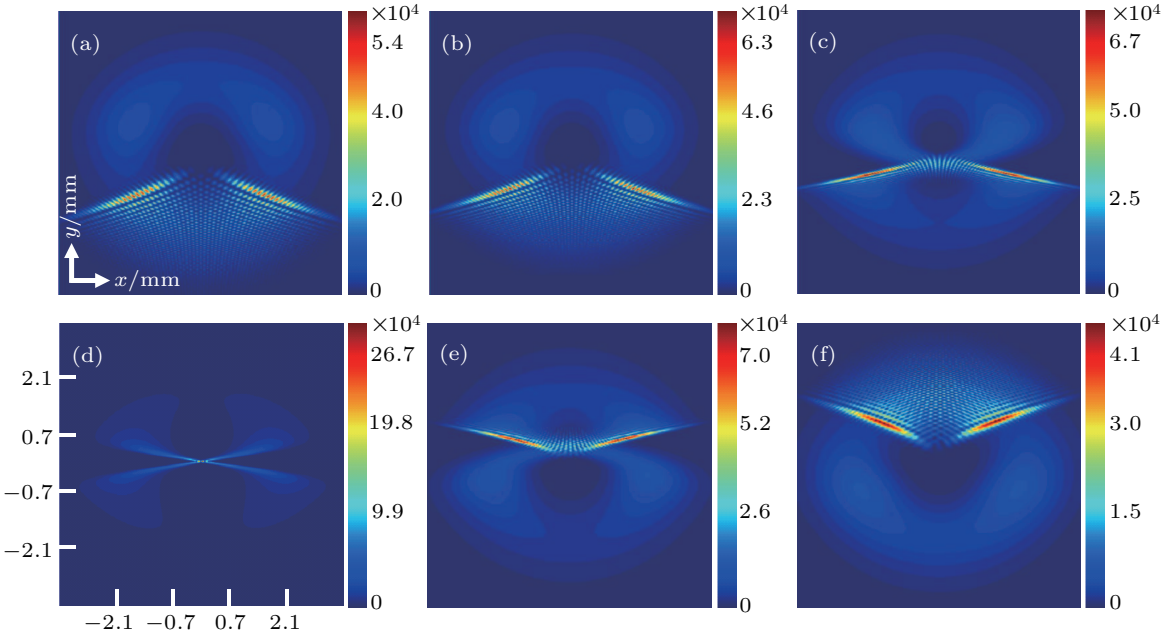


Fig. 1. Synthesizing intensity distribution as the RPPGVB travels along the z-axis in free space with parameters: $\lambda = 500$ nm, $x_d = y_d = 0$, $x' = y' = 0.1$ mm, $w_0 = 2$ mm: (a) $z = 0$, (b) $z = 0.3z_e$, (c) $z = 0.8z_e$, (d) $z = z_e$, (e) $z = 1.2z_e$, (f) $z = 1.8z_e$. The unit of the intensity in all the figures is cd.

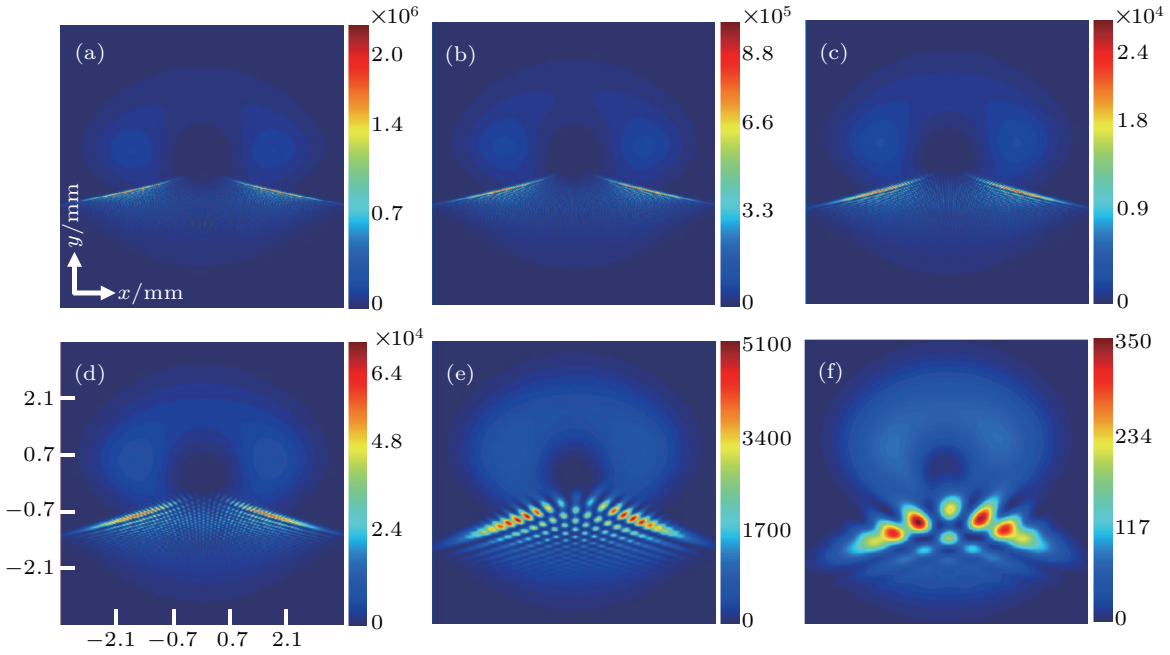


Fig. 2. Synthesizing intensity at $z = 0.5z_e$ when changing the values of x' and y' with parameters $\lambda = 500$ nm, $n_o = n_e = 1$, $x_d = y_d = 0$, $w_0 = 2$ mm: (a) $x' = y' = 0.04$ mm, (b) $x' = y' = 0.05$ mm, (c) $x' = y' = 0.07$ mm, (d) $x' = y' = 0.1$ mm, (e) $x' = y' = 0.2$ mm, (f) $x' = y' = 0.4$ mm.

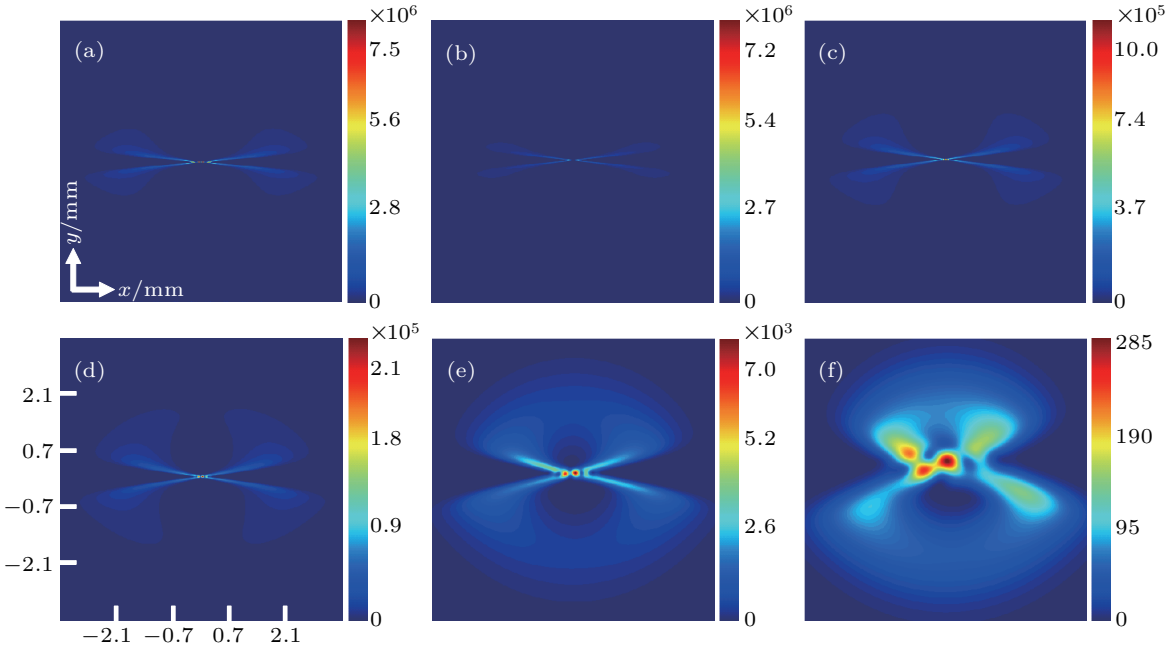


Fig. 3. Synthesizing intensity at $z = z_e$ when changing the values of x' and y' with parameters $\lambda = 500$ nm, $x_d = y_d = 0$, $w_0 = 2$ mm: (a) $x' = y' = 0.04$ mm, (b) $x' = y' = 0.05$ mm, (c) $x' = y' = 0.07$ mm, (d) $x' = y' = 0.1$ mm, (e) $x' = y' = 0.2$ mm, (f) $x' = y' = 0.4$ mm.

Figure 5 demonstrates the intensity at $z = 0$ when the values of x_d and y_d are changed. From Figs. 5(a) and 5(b), we find that a part of the RPPGVB's lobes disappear when $x < 0$, which means that there is a vortex at that position. From Figs. 5(a)–5(c), we find that the vortex moves at an angle to the positive x-direction. The energy of the RPPGVB mainly distributes on the lobes at $x > 0$. The main part of the facula appears at $x > 0$ and $x_d = y_d < 0$ in Figs. 5(a) and 5(b), and the peak intensity tends to decrease with the increase of the displacement. When x_d and y_d equal 0, as shown in Fig. 5(c), the number of the faculae is two and the vortex just locates at the center of the RPPGVB's profile. What's more, the whole cross section is symmetric about $x = 0$. The missing part of the lobe pattern reappears as well. When x_d and y_d are farther than zero, the energy mostly transfers to the lobes at $x < 0$ and the facula at $x > 0$ disappears. What's more, the peak intensity increases when x_d and y_d get larger positive values, as shown in Figs. 5(d)–5(f).

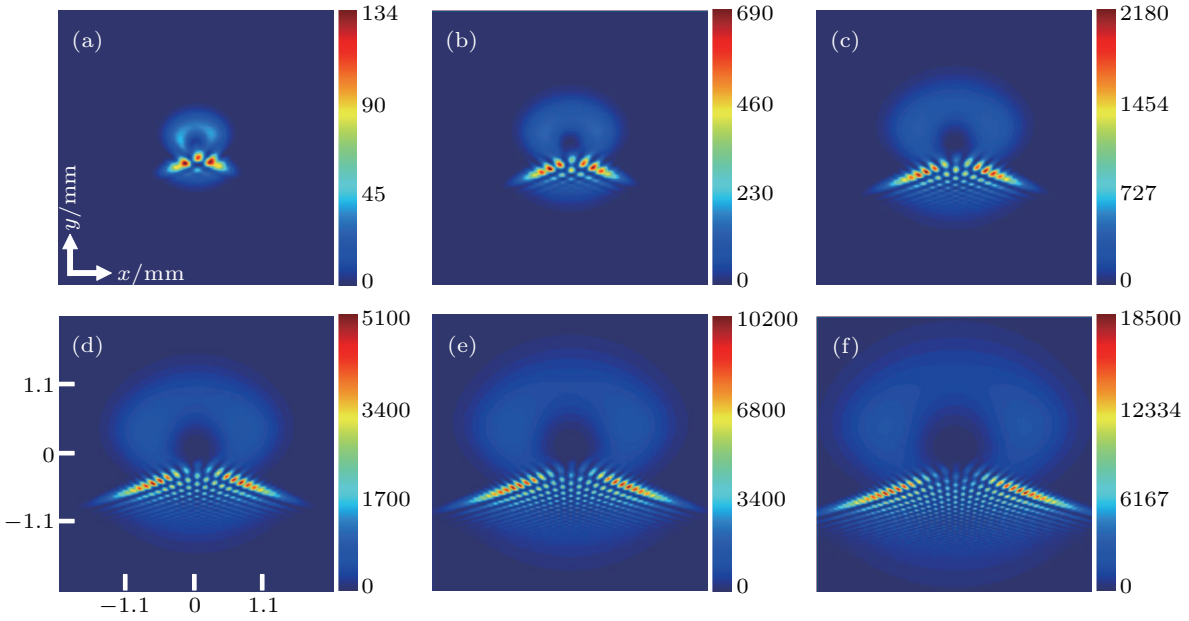


Fig. 4. Synthesizing intensity at $z = 0.5z_e$ when changing the value of w_0 with parameters $\lambda = 500$ nm, $x_d = y_d = 0$, $x' = y' = 0.1$ mm: (a) $w_0 = 0.4$ mm, (b) $w_0 = 0.6$ mm, (c) $w_0 = 0.8$ mm, (d) $w_0 = 1$ mm, (e) $w_0 = 1.2$ mm, (f) $w_0 = 1.4$ mm.

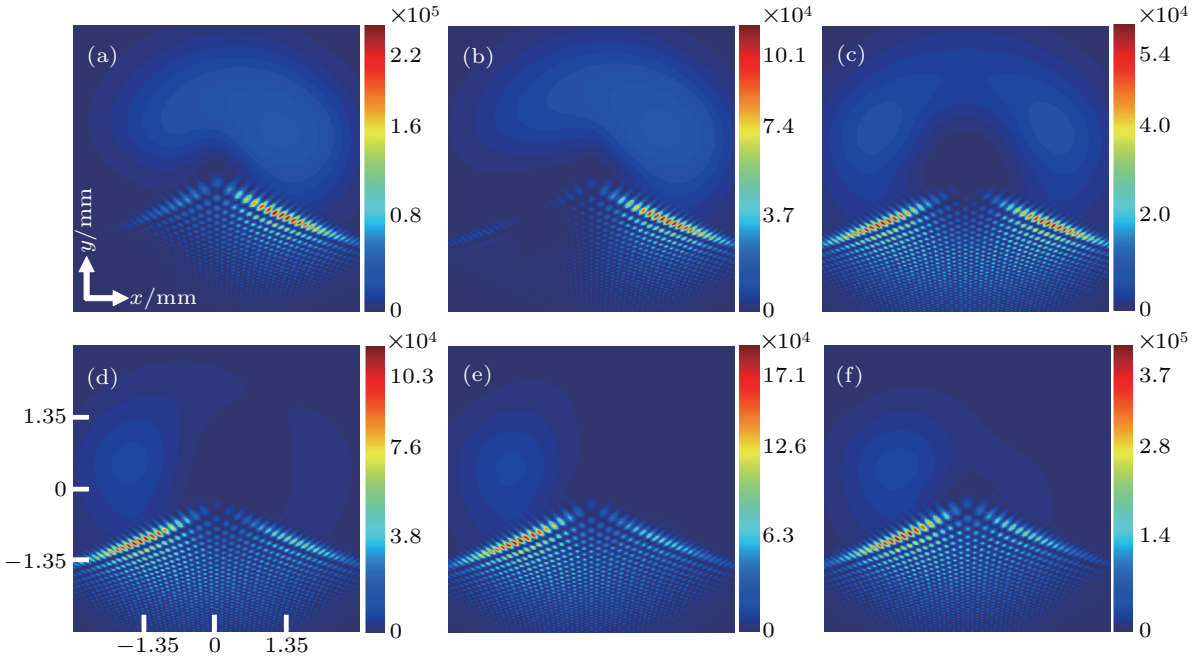


Fig. 5. Intensity at $z = 0$ when changing the values of x_d and y_d with other parameters $\lambda = 500$ nm, $x' = y' = 0.1$ mm, $w_0 = 2$ mm: (a) $x_d = y_d = -2$ mm, (b) $x_d = y_d = -1$ mm, (c) $x_d = y_d = 0$ mm, (d) $x_d = y_d = 0.5$ mm, (e) $x_d = y_d = 1$ mm, (f) $x_d = y_d = 2$ mm.

Through the previous investigations, we have learned the RPPGVB will focus on the point $z = z_e$ and the scaling factor y' is much smaller than the waist radius w_0. From Figs. 6(a)–6(f), we find that there is always a focal point at the center of the profile. What's more, the faculae assume different shapes when x_d and y_d get changed. When x_d and y_d are less than zero, there are two vortexes at the cross section. When the values of x_d and y_d increase to zero, as shown in Fig. 6(c), four faculae arise and the whole beam's profile is symmetric about the x-axis and the y-axis. When x_d and y_d keep increasing, the faculae shrink at $x > 0$.

For the intensity, the peak intensity occurs at the focal point and its value decreases at first and then grows when x_d and y_d increase to zero. When $x_d > 0$ and $y_d > 0$ with the increase of x_d and y_d, the peak intensity will become larger and larger, which is revealed by Figs. 6(d)–6(f).

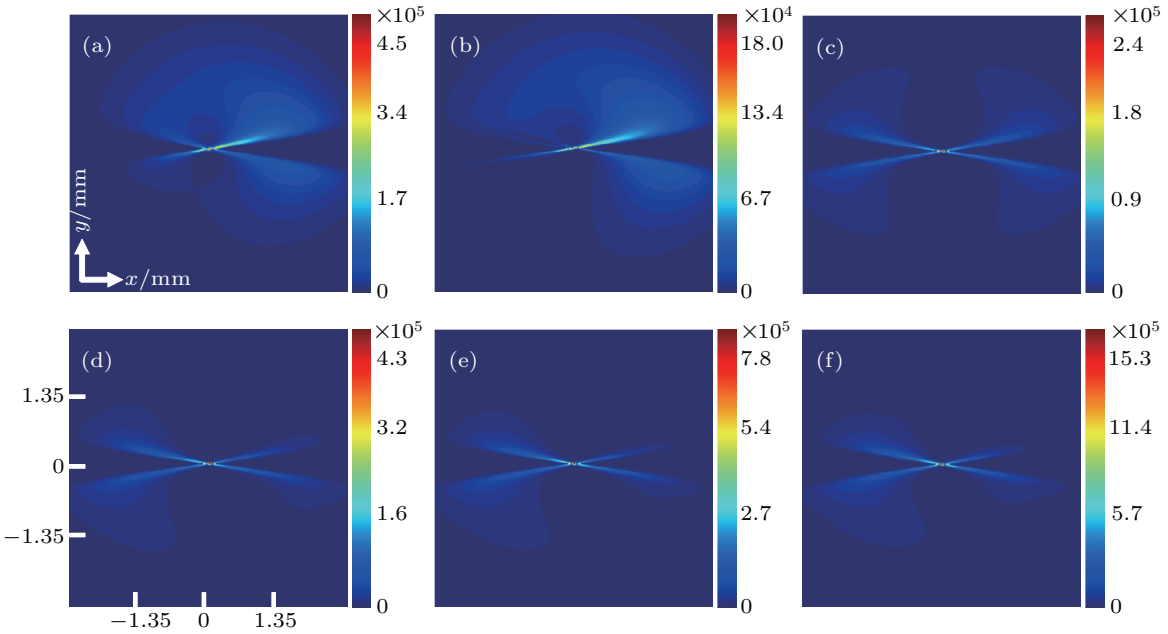


Fig. 6. All are the same as those in Fig. 5 except $z = z_e$.

Figures 7 and 8 show the phases of the x and the y components of the RPPGVB at different propagation distances. The equiphase zones are narrow bands and the boundaries between them are more orderly at $z = 0$ than those at other distances for both E_x and E_y. What's more, there is a clear boundary at $x = 0$ and $z = 0$ in Fig. 7(a) and the phase is abrupt when it crosses this boundary, which makes the overall phase distribution asymmetrical. Similarly, there is a boundary at $y = 0$ for E_y at the initial plane from Fig. 8(a). Another attractive point is that the isophase band bends at the boundary of the lobe zone at $z = 0$, which cannot be found in other phase patterns. When we turn our attention to other positions, we find that the phase distribution diagrams at other planes for E_x and E_y are funnel-shaped. Furthermore, the phase boundary at $x = 0$ is less obvious than that in the same plane for E_x. In addition, we can learn from Figs. 8(b)–8(f) that funnel graphs are basically symmetric along $x = 0$ in each figure of E_y except Fig. 8(d). When the RPPGVB propagates at $z = z_e$, two equiphase zones appear obviously near $y = 0$ for E_x and E_y. The phases of the two regions equal -0.5 rad for E_x while the phases of the left and right parts are equal to 2.5 rad and -0.5 rad, respectively, for E_y.

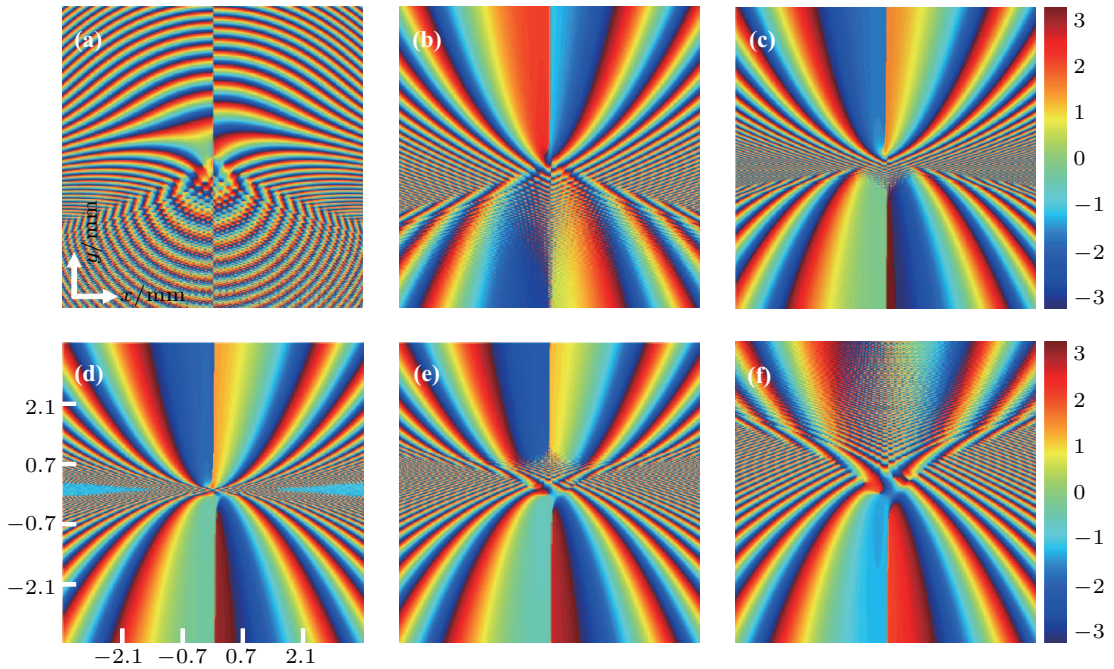


Fig. 7. Phase distribution of E_x when the RPPGVB propagates along the z-direction. Parameters are the same as those in Fig. 1 and the unit of phase is rad.

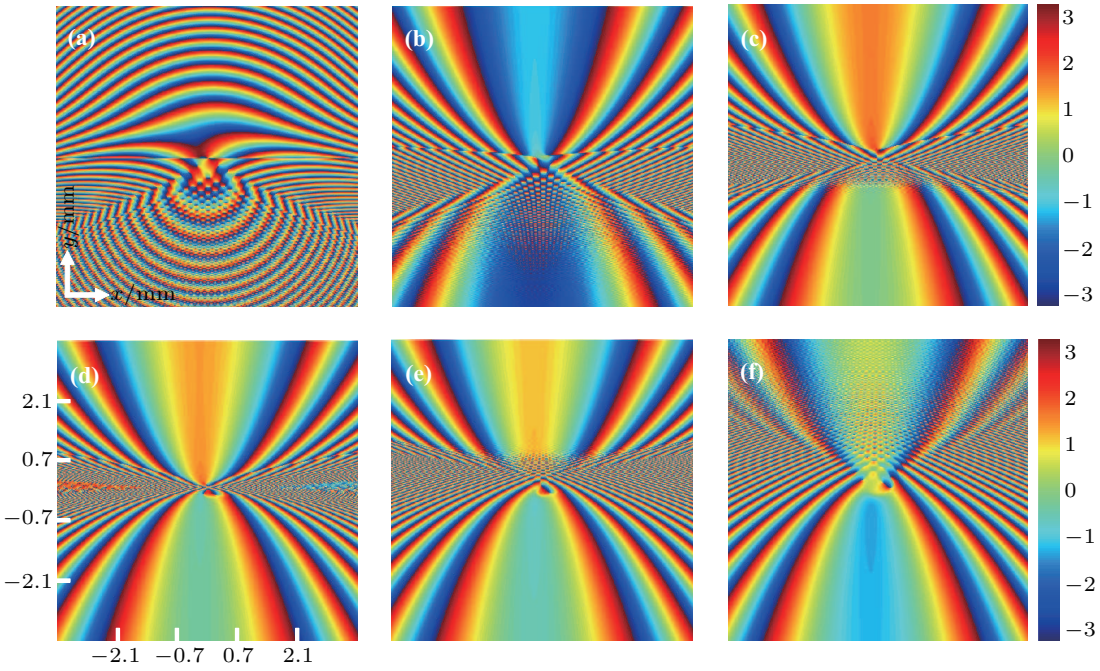


Fig. 8. The same as Fig. 7 but E_y.

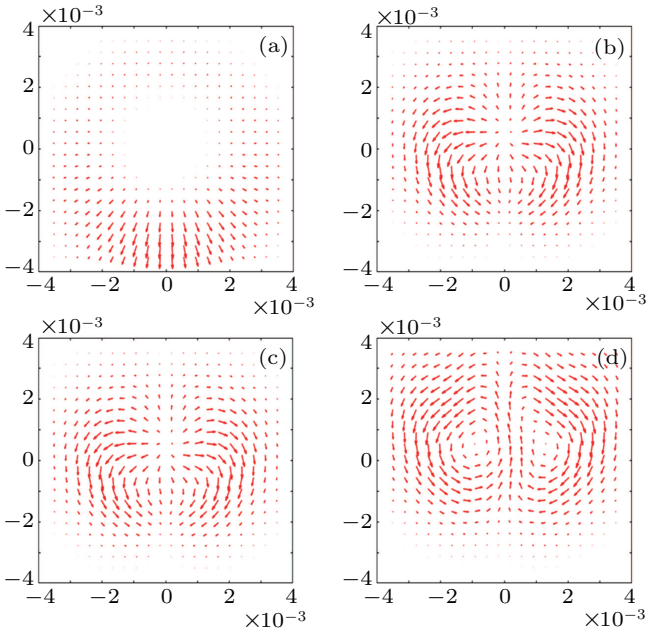


Fig. 9. Spin currents at different planes as the RPPGVB propagates along the z-direction. Parameters are the same as those in Fig. 1 except (a) $z = 0$, (b) $z = 0.8z_e$, (c) $z = z_e$, (d) $z = 1.8z_e$. The lengths and directions of the arrows represent the normalized sizes and directions of the spin currents.

Figure 9 shows the spin currents at different planes when the RPPGVB propagates along the z-direction in free space. At $z = 0$, the sizes of spin currents in the central area are zero but the ones in other area are not and point at all directions regularly. Figures 9(b) and 9(c) show the spin currents at $z = 0.8z_e$ and z_e. We find that they are similar to each other. Spin current vectors at the central area point around, while the surrounding ones have a tendency to point toward the positive direction of the y-axis. In addition, spin current vectors which are away from $x = 0$ are larger than those near $x = 0$ in size. When z equals $1.8z_e$, there are two small areas whose shapes are like vortices on both sides of $x = 0$. The spin currents around $x = 0$ roughly point to the positive direction of the y-axis.

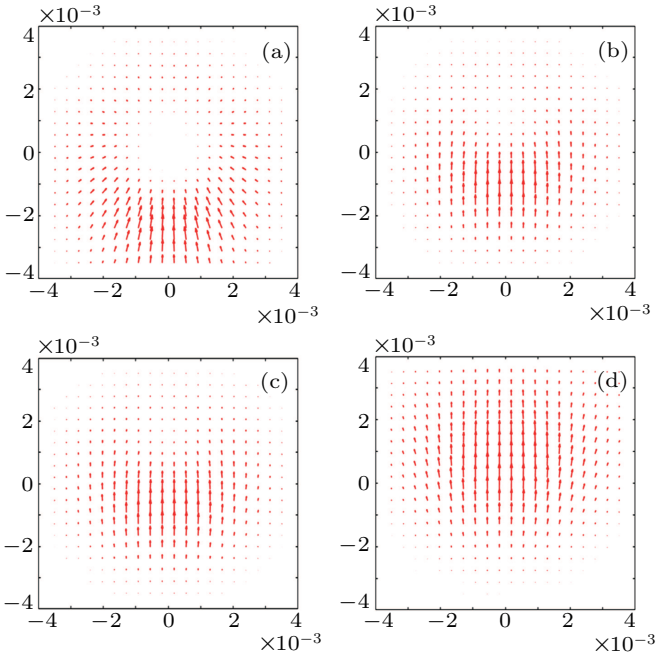


Fig. 10. All parameters are the same as those in Fig. 9 except the orbital currents of the RPPGVB. The lengths and directions of the arrows represent the normalized sizes and directions of the orbital currents.

Figure 10 presents the orbital currents of the RPPGVB as it propagates along the z-direction. At $z = 0$, sizes of orbital currents around the central part equal zero. Contrary to spin currents, the orbital currents everywhere point at the center of the figure at $z = 0$. When z equals $0.8z_e$ and z_e,

nearly all orbital currents point to the positive direction of the y-axis. Large orbital currents gather in the region where -2 mm $\leq x \leq 2$ mm and -2 mm $\leq y \leq 0$. When z continues to increase, the orbital currents in the upper part of the image and the gathered area of orbital currents become larger. When z equals $1.8z_e$, the area extends to -2.5 mm $\leq x \leq 2.5$ mm and -1.7 mm $\leq y \leq 2.8$ mm. All of the orbital currents still point at the positive direction of the y-axis.

4. Conclusion

We have introduced a new type of beam named as the RPPGVB and studied its propagation properties. Although all parameters have effects on the RPPGVB's intensity pattern and the energy distribution, the main roles they play are different. For example, the scaling factors mainly affect the value of the intensity but have few effects on the intensity distribution. When enlarging the radius of the RPPGVB's waist, the area of the RPPGVB's cross-section expands accordingly, whereas the relative intensity distribution changes a little. The displacements of the vortex mainly influence the energy distribution and the shape of patterns of the RPPGVB. The spin currents and orbital currents of the RPPGVB are researched as well. We find that with the increase of the propagation distance, the spin currents tend to form two vortices at the center of the RPPGVB's profile while the orbital currents gradually point at a specific direction orderly. Our investigation will provide a better understanding about the state of the RPPGVB propagating in vacuum and be useful for applications in information transmission.

References

[1] Gahagan K T and Swartzlander G A 1996 *Opt. Lett.* **21** 827
[2] Gbur G and Tyson R K 2008 *J. Opt. Soc. Am. A* **25** 225
[3] Ng J, Lin Z and Chan C T 2010 *Phys. Rev. Lett.* **104** 103601
[4] Soskin M S, Gorshkov V N, Vasnetsov M V, Malos J T and Heckenberg N R 1997 *Phys. Rev. A* **56** 4064
[5] Carpentier A V, Michinel H, Salgueiro J R and Olivieri D 2008 *Am. J. Phys.* **76** 916
[6] Yi X N, Ling X H, Zhang Z Y, Li Y, Zhou X X, Liu Y C, Chen S Z, Luo H L and Wen S C 2014 *Opt. Express* **22** 17207
[7] Masajada J and Dubik B 2001 *Opt. Commun.* **198** 21
[8] Li P, Zhang Y, Liu S, Ma C J, Han L, Cheng H C and Zhao J L 2016 *Opt. Lett.* **41** 2205
[9] Lee W M, Yuan X C and Cheong W C 2004 *Opt. Lett.* **29** 1796
[10] Vaity P and Rusch L 2015 *Opt. Lett.* **40** 597
[11] Simpson N B, Dholakia K, Allen L and Padgett M J 1997 *Opt. Lett.* **22** 52
[12] Paterson C 2005 *Phys. Rev. Lett.* **94** 153901
[13] Grier D G 2003 *Nature* **424** 810
[14] Chen Y H, Wang F, Zhao C L and Cai Y J 2014 *Opt. Express* **22** 5826
[15] Grosjean T, Courjon D and Spajer M 2002 *Opt. Commun.* **203** 1
[16] Dorn R, Quabis S and Leuchs G 2003 *Phys. Rev. Lett.* **91** 233901
[17] Niziev V G and Nesterov A V 1999 *J. Phys. D: Appl. Phys.* **32** 1455
[18] Machavariani G, Lumer Y, Moshe I, Meir A and Jackel S 2007 *Opt. Lett.* **32** 1468
[19] Lerman G M and Levy U 2008 *Opt. Lett.* **33** 2782
[20] Yonezawa K, Kozawa Y and Sato S 2006 *Opt. Lett.* **31** 2151
[21] Berry M V and Balazs N L 1979 *Am. J. Phys.* **47** 264
[22] Lin Y, Seka W, Eberly J H, Huang H and Brown D L 1992 *Appl. Opt.* **31** 2708
[23] Lin J, Dellinger J, Genevet P, Cluzel B, de F and Capasso F 2012 *Phys. Rev. Lett.* **109** 093904
[24] Ring J D, Lindberg J, Mourka A, Mazilu M, Dholakia K and Dennis M R 2012 *Opt. Express* **20** 18955
[25] Deng D M, Chen C D, Zhao X, Chen B, Peng X and Zheng Y S 2014 *Opt. Lett.* **39** 2703
[26] Ren Z J, Fan C J, Shi Y L and Chen B 2016 *J. Opt. Soc. Am. A* **33** 1523
[27] Cheng K, Lu G and Zhong X 2017 *Appl. Phys. B* **123** 60
[28] Pearcey T 1946 *London Edinburgh Dublin Philos. Mag. J. Sci.* **37** 311
[29] Ciattoni A and Palma C 2003 *J. Opt. Soc. Am. A* **20** 2163
[30] Xu C J, Lin L D, Huang Z Z, Chen Y Z, Yang X B, Liu H Z and Deng D M 2018 *Laser Phys.* **28** 115001